

# Asteroseismic analysis of the roAp star $\alpha$ Circini: 84 days of high-precision photometry from the *WIRE* satellite\*

H. Bruntt<sup>1</sup>, D. W. Kurtz<sup>2</sup>, M. S. Cunha<sup>3</sup>, I. M. Brandão<sup>3,4</sup>, G. Handler<sup>5</sup>, T. R. Bedding<sup>1</sup>, T. Medupe<sup>6,7</sup>, D. L. Buzasi<sup>8</sup>, D. Mashigo<sup>6</sup>, I. Zhang<sup>6</sup>, F. van Wyk<sup>7</sup>

<sup>1</sup>*Sydney Institute for Astronomy, School of Physics A29, University of Sydney, 2006 NSW, Australia*

<sup>2</sup>*Jeremiah Horrocks Institute of Astrophysics and Supercomputing, University of Central Lancashire, Preston PR1 2HE, UK*

<sup>3</sup>*Centro de Astrofísica da Universidade do Porto, Rua das Estrelas, 4150-Porto, Portugal*

<sup>4</sup>*Departamento de Matemática Aplicada, Faculdade de Ciências, Universidade do Porto, 4169 Porto, Portugal*

<sup>5</sup>*Institut für Astronomie, Universität Wien, Türkenschanzstrasse 17, A-1180 Wien, Austria*

<sup>6</sup>*Department of Astronomy, University of Cape Town, Rondebosch 7700, South Africa*

<sup>7</sup>*South African Astronomical Observatory, P.O. Box 9, Observatory 7935, South Africa*

<sup>8</sup>*Department of Astronomy, University of Washington, Seattle WA 98195, USA*

Accepted XXX; Received YYY; in original form ZZZ

## ABSTRACT

We present a detailed study of the pulsation of  $\alpha$  Circini, the brightest of the rapidly oscillating Ap stars. We have obtained 84 days of high-precision photometry from four runs with the star tracker on the *WIRE* satellite. Simultaneously, we collected ground-based Johnson *B* observations on 16 nights at the South African Astronomical Observatory. In addition to the dominant oscillation mode at  $2442 \mu\text{Hz}$ , we detect two new modes that lie symmetrically around the principal mode to form a triplet. The average separation between these modes is  $\Delta f = 30.173 \pm 0.004 \mu\text{Hz}$  and they are nearly equidistant with the separations differing by only  $3.9 \text{ nHz}$ . We compare the observed frequencies with theoretical pulsation models based on constraints from the recently determined interferometric radius and effective temperature, and the recently updated *Hipparcos* parallax. We show that the theoretical large separations for models of  $\alpha$  Cir with global parameters within the  $1 \sigma$  observational uncertainties vary between  $59$  and  $65 \mu\text{Hz}$ . This is consistent with the large separation being twice the observed value of  $\Delta f$ , indicating that the three main modes are of alternating even and odd degrees. The frequency differences in the triplet are significantly smaller than those predicted from our models, for all possible combinations of mode degrees, and may indicate that the effects of magnetic perturbations need to be taken into account. The *WIRE* light curves are modulated by a double wave with a period of  $4.479 \text{ d}$ , and a peak-to-peak amplitude of  $4 \text{ mmag}$ . This variation is due to the rotation of the star and is a new discovery, made possible by the high precision of the *WIRE* photometry. The rotational modulation confirms an earlier indirect determination of the rotation period. The main pulsation mode at  $2442 \mu\text{Hz}$  has two sidelobes split by exactly the rotation frequency. From the amplitude ratio of the sidelobes to the central peak we show that the principal mode is consistent with an oblique axisymmetric dipole mode ( $l = 1, m = 0$ ), or with a magnetically distorted mode of higher degree with a dominant dipolar component.

**Key words:** stars: individual:  $\alpha$  Cir – stars: oscillations – stars: rotation – stars: fundamental parameters – stars: variables: other

## 1 INTRODUCTION

$\alpha$  Circini (HR 5463, HD 128898, HIP 71908;  $V = 3.2$ ) is the brightest of the rapidly oscillating chemically peculiar A-type (roAp) stars (see reviews by Kurtz & Martinez 2000 and

Kurtz et al. 2004). It was among the first of the class to be discovered (Kurtz 1982), showing photometric variations with a period  $P_{\text{pul}} = 6.8 \text{ min}$  and an amplitude of a few mmag in Johnson *B* (Kurtz & Cropper 1981). The multi-site photometric campaign by Kurtz et al. (1994) revealed four low amplitude modes in addition to the main mode. The roAp stars pulsate in high overtones and are described by the oblique pulsator model

\* Based on observations at the South African Astronomical Observatory.

**Table 1.** List of photometric observations from the *WIRE* satellite and the 0.5-m and 0.75-m telescopes at SAAO. In the last column we list the point-to-point scatter ( $\sigma$ ) in the time series.

Source	Observing dates	$T_{\text{obs}}$ [days]	Data points	$\sigma$ [mmag]
<i>WIRE</i>	2000 Aug. 18–Sep. 29	42.2	39 479	0.93
–	2005 Feb. 16–25	8.3	10 857	1.04
–	2006 Feb. 10–Mar. 15	31.0	29 616	0.91
–	2006 July 7–31	24.3	27 273	0.61
SAAO	2006 Feb. 7–Feb. 19	12.0	1 802	2.4
–	2006 June 23–July 24	31.2	2 330	2.0

(Kurtz 1982; Shibahashi & Takata 1993; Takata & Shibahashi 1995; Bigot & Dziembowski 2002; Saio 2005). In this model the magnetic axis is inclined to the rotation axis. The oscillation modes follow the magnetic field, therefore the deformation of the star is observed from different perspectives. This was observed in  $\alpha$  Cir by Kurtz et al. (1994), who found a significant modulation of the amplitude of the main mode, making it possible to determine the rotation period to be  $P_{\text{rot}} = 4.4790 \pm 0.0001$  d.

Simultaneous excitation of several high-order modes in roAp stars makes them ideal targets for detailed asteroseismic studies. Asymptotic theory predicts a regular pattern of frequencies, dominated by the large separation, which depends mainly on the mean density of the star. Asteroseismology of roAp stars makes it possible to probe their internal properties, including aspects of the structure and magnetic fields (Cunha et al. 2003). Previous detailed studies of multi-mode roAp stars have in some cases been limited because the fundamental parameters are poorly known (e.g. Cunha et al. 2007). For example, the effective temperature determined from different photometric indices or spectroscopic analyses typically give results spanning 500 K or more (Netopil et al. 2008). This large range may be explained, in part, by the chemical peculiarities and strong magnetic fields in roAp stars, resulting in heavy line blanketing in some regions of the spectra. Matthews et al. (1999) presented observational evidence of systematic errors in the effective temperatures of a dozen roAp stars, based on the measurements of their large separations.

In our companion paper (Bruntt et al. 2008, Paper I), we used interferometric measurements with the Sydney University Stellar Interferometer (SUSI) to determine the radius of  $\alpha$  Cir. Combined with a determination of the bolometric flux from calibrated spectra, we found the temperature to be  $7420 \pm 170$  K. Unlike previous determinations of  $T_{\text{eff}}$ , which range from 7670 to 8440 K, our determination is nearly independent of atmospheric models – only the limb-darkening correction depends on the adopted grid of model atmospheres, and weakly so.

Here we report observations of  $\alpha$  Cir, made simultaneously with the *WIRE* satellite and from the ground. The high-precision satellite photometry has allowed us to detect the large separation in  $\alpha$  Cir for the first time. This new result, combined with the constraints on the radius and  $T_{\text{eff}}$  from Paper I, allow us to make an asteroseismic investigation based on theoretical models.

## 2 OBSERVATIONS

Soon after the launch of the *WIRE* satellite on 4 March 1999, the hydrogen coolant for the main infrared camera was lost. However,

**Table 2.** List of photometric observations from the 0.5-m and 0.75-m telescopes at SAAO. The first and second columns give the initials of the observer and the telescope used. The duration in the fourth column is from start to end of observations for each night which sometimes includes gaps due to poor weather. The fifth column gives the number of averaged 40-s integrations obtained and the last column is the standard deviation of one observation with respect to the mean for the night.

Obs.	Tel	Date 2006	$T_{\text{obs}}$ [h]	Data points	$\sigma$ [mmag]
GH	0.5-m	07–08 Feb.	0.58	49	3.5
GH	0.5-m	12–13 Feb.	0.95	83	3.4
GH	0.75-m	13–14 Feb.	3.04	258	1.8
GH	0.5-m	13–14 Feb.	0.45	40	2.0
GH	0.75-m	14–15 Feb.	3.97	341	2.4
GH	0.75-m	15–16 Feb.	2.58	224	1.8
GH	0.75-m	16–17 Feb.	3.95	264	2.3
GH	0.75-m	17–18 Feb.	3.49	302	2.7
GH	0.75-m	19–20 Feb.	2.88	241	2.5
total			21.89	1802	
DM	0.5-m	23–24 Jun.	5.45	381	2.0
DM	0.5-m	24–25 Jun.	5.45	445	1.7
DM	0.5-m	07–08 Jul.	5.22	418	1.9
DM	0.5-m	11–12 Jul.	3.89	88	2.1
DM	0.5-m	17–18 Jul.	4.79	396	1.8
DM	0.5-m	18–19 Jul.	4.79	389	2.0
IZ	0.5-m	24–25 Jul.	4.16	213	1.9
total			33.75	2330	

the star tracker was used to observe around 240 stars with apparent magnitudes  $V < 6$  until communication with the satellite failed on 2006 October 23 (Buzasi 2002; Bruntt 2007; Bruntt & Southworth 2008). The 52 mm aperture illuminated a SITe CCD camera and windows centered on the five brightest stars in the field were acquired at a cadence of 2 Hz. Each *WIRE* field was typically monitored for 2 to 4 weeks and some targets, including  $\alpha$  Cir, were observed in more than one season. *WIRE* switched between two targets during each orbit in order to best avoid the illuminated face of the Earth. Consequently, the duty cycle was typically around 20 to 40 percent, or about 19 to 38 minutes of continuous observations per orbit. The time baseline of the observations analysed here is almost six years, during which the orbital period of the satellite decreased from 96.0 to 93.3 minutes.

The roAp star  $\alpha$  Cir was observed during four runs with *WIRE*. The first data set in 2000 September was not optimal in that several long gaps are present and the sub-pixel position on the CCD was less stable than the succeeding runs. The second run in 2005 February lasted 8 days, and was followed by runs of 31 and 24 days in 2006 February and July. A log of the observations is given in Table 1. Excluding the gaps in the time series,  $\alpha$  Cir was observed for 84 days, making it one of the most observed stars with *WIRE*.

To be able to compare the *WIRE* results with previous ground-based studies, we collected additional ground-based photometric time-series. During both runs with *WIRE* in 2006 we made simultaneous photometric observations in the Johnson  $B$  filter from the South African Astronomical Observatory (SAAO). We used the Modular Photometer on the 0.5-m telescope and the University of Cape Town Photometer on the 0.75-m telescope. All observations were made through a Johnson  $B$  filter, plus a neutral density filter of 2.3 mag on the 0.5-m telescope and 5 mag on the 0.75-m telescope. The neutral density filters were needed to keep the count

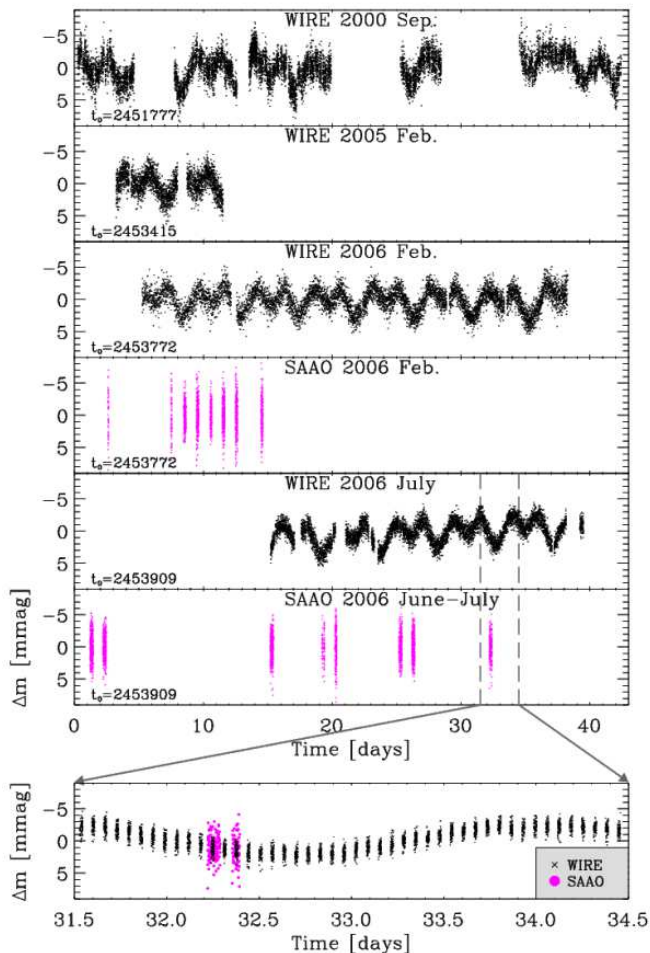


**Figure 1.** The four light curves of  $\alpha$  Cir from *WIRE* and the two light curves from SAAO. The different zero points in time are indicated in each panel. The *bottom panel* shows an expanded view of three days where simultaneous observations with *WIRE* and SAAO were made.

rates for this very bright star at levels that would not damage the photomultiplier tubes, or result in large dead-time corrections. The resultant count rates were about  $380\,000\text{ s}^{-1}$  for the 0.5-m telescope and  $150\,000\text{ s}^{-1}$  for the 0.75-m telescope. A detailed log of the observations from SAAO is given in Table 2.

The light curves from *WIRE* and SAAO are shown in Fig. 1. The *bottom panel* shows an expanded view of simultaneous observations. In each panel we give the time zero point  $t_0$  as the Heliocentric Julian Date (HJD).

## 2.1 Data reduction

The *WIRE* data set consists of 3.3 million windows extracted by the on-board computer from the  $512 \times 512$  pixels CCD star tracker camera. Each window is  $8 \times 8$  pixels and aperture photometry was carried out using the pipeline described by Bruntt et al. (2005). The data collected within 15 seconds are binned to decrease the number of data points to 107 225 (cf. Table 1). We note that  $\alpha$  Cir is a visual binary with a separation of  $15''.6$ . Since the pixel size of the *WIRE* CCD is  $60''$ , the B component is entirely within the applied photometric aperture. As noted by Kurtz et al. (1994) the contamination is negligible, since the difference in magnitude is  $\Delta V = 5.05$ . With the Strömgren indices of the B-component from

Sinachopoulos (1989) and using the TEMPLOGG software (Rogers 1995; Kupka & Bruntt 2001) for the calibration, we find  $T_{\text{eff}} \simeq 4660 \pm 200\text{ K}$ ,  $\log g = 4.6 \pm 0.2$ , and  $[\text{Fe}/\text{H}] = -0.26 \pm 0.10$ , suggesting that it is a K5 V star. In the following, we use  $\alpha$  Cir to mean the A component of the system.

The raw light curves contain a small fraction (1 to 10%) of outlying data points. These points were identified and removed based on the measured position, background level, and width of the stellar image (PSF). The light curves from Sep'00, Feb'05 and Feb'06 have a high amount of scattered light towards the end of each orbit, increasing the background level from about 20 to 1400 ADU. In these light curves we found a significant correlation between the background and the measured flux, which we removed by a spline fit. The light curve from Jul'06 has low background, and in this case we found a correlation of the measured flux and the width of the PSF, which was removed by subtracting a second-order polynomial.

The SAAO data were obtained in high-speed mode using continuous 10-s integrations. With continuous observations of the target star, no comparison stars were observed. Sky observations were made as needed, based on conditions throughout the observing run. The data were corrected for dead-time losses, sky subtracted and the mean extinction was removed. They were then averaged four points at a time into 40-s integrations. Some remaining low frequency variability, caused by transparency variations, was removed with high-pass filtering that did not affect the pulsation frequencies of interest in the data. This latter step results in white noise across the frequency spectrum, and hence better estimates of errors on amplitudes and phases than would be the case if low frequency variance were left in the data. The last column of Table 2 gives the standard deviation for each night of observations. The contribution to the standard deviation from the actual pulsations is small, so it is a good measure of the quality of the night. On some nights, weather interruptions resulted in gaps in the data, which is reflected in the number of data points and duration of each night in Table 2.

## 3 LIGHT CURVE ANALYSIS

The light curves of  $\alpha$  Cir show variations on two different time scales. The double wave seen in the *WIRE* data in Fig. 1 has a period of 4.479 d and is due to rotation, seen here for the first time, while the periods of the rapid oscillations lie in the range 6.5 to 7.0 min, or three orders of magnitude faster. In the following Sections we will analyse these variations in detail.

### 3.1 Rotational period and inclination angle

To measure the rotation period, we fitted the observed double wave with two sinusoids with frequencies  $f_A$  and  $f_B = 2 \times f_A$ , yielding a period of  $P_{\text{rot}} = 4.4792 \pm 0.0004\text{ d}$ . In this analysis we first subtracted the high-frequency oscillations (see Sect. 3.2). In Fig. 2 we show the binned lights curves from Feb'06 and Jul'06, phased with the rotation period with a zero point in time  $t_{\text{rot}} = \text{HJD}245\,3937.2086$ . The peak-to-peak variation is only about 4 mmag and it is the excellent precision and low frequency stability of the *WIRE* data that have allowed us to make the first direct measurement of the rotation of  $\alpha$  Cir. Ground-based observations have not been able to do this, partly because of the low amplitude of the variations and partly because of the challenge of making differential photometric observations on such a bright star.

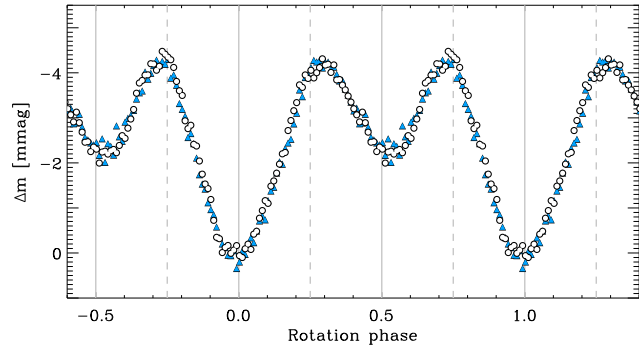


**Figure 2.** Binned light curves of  $\alpha$  Cir from *WIRE* phased with the rotation period. Triangle symbols are data from Feb'06 and circles are from Jul'06. Vertical lines are shown to guide the eye. The zero point in time for the phase is  $t_{\text{rot}} = \text{HJD}245\,3937.2086$ .

From the rotation period and the interferometrically determined radius of  $R/R_{\odot} = 1.967 \pm 0.066$  (Paper I), we find the rotational velocity to be  $v_{\text{rot}} = 21.4 \pm 0.7 \text{ km s}^{-1}$ . We can thus estimate the inclination of the rotation axis from the measured  $v \sin i$ . The average value from Kupka et al. (1996) and Balona & Laney (2003) is  $v \sin i = 13.0 \pm 1.5 \text{ km s}^{-1}$ . A more accurate value has been determined from spectra collected with the UVES spectrograph:  $v \sin i = 13.0 \pm 1.0 \text{ km s}^{-1}$  (Vladimir Elkin, private communication). These UVES spectra have better resolution and higher S/N than previous studies, thus we use this value of  $v \sin i$  to determine the inclination to be  $i = 37 \pm 4^{\circ}$ .

The rotation of  $\alpha$  Cir was first measured indirectly by Kurtz et al. (1994) from the amplitude modulation of the principal oscillation mode at  $2442 \mu\text{Hz}$ . From the observed frequency separation of the two symmetrical side-lobes, Kurtz et al. (1994) determined the period  $P_{\text{rot}} = 4.463 \pm 0.010 \text{ d}$ . This was refined to get  $P_{\text{rot}} = 4.4790 \pm 0.0001$  using photometry from several observing campaigns with a baseline of 12 y (Kurtz et al. 1994). These results are in very good agreement with our direct measurement.

We interpret the modulation of the light curves in Fig. 2 as being due to surface features, most likely two spots of over-abundances of rare earth elements located near the equator, thus not associated with the magnetic and pulsation poles. Such spots are typical of the  $\alpha^2$  CVn class of photometrically variable magnetic Ap stars (see, e.g., Pyper 1969). Redistribution of flux from blue to red because of the increased line blanketing in the blue often gives rise to rotational light variations that are out-of-phase between blue- and red-filter observations in Ap stars. We cannot determine with certainty whether this is the case for  $\alpha$  Cir, as we have only very broad-band observations with *WIRE* with an uncertain filter function (see section 3.4). Since the flux from the star is dominated by blue light, given that  $T_{\text{eff}} = 7420 \pm 170 \text{ K}$  (Paper I), it is likely that the double wave variation shows minima when each spot is closest to the line-of-sight. The two spots are of different size, hence giving the double wave variation with rotation. We note that the double wave is asymmetrical (as can be seen in Fig. 2), since the secondary minimum lies at phase  $0.519 \pm 0.008$ . It is worth noting that the configuration of the spots that give rise to the rotational light modulation did not appear to change significantly during any of the runs with *WIRE*. We will discuss the spot configuration in more detail in a future publication concerning Doppler imaging of the rotational light curve.

Measurements of the magnetic field of  $\alpha$  Cir are inconclusive regarding its variability with the rotation period. Bychkov et al.

**Table 3.** Frequencies extracted from the two combined *WIRE* data sets from 2006. Three frequencies were fitted to the SAO *B*-filter photometry as described in the text. The phases are with respect to  $t_0 = \text{HJD}245\,3939$ .

ID	WIRE			SAAO	
	$f$ [ $\mu\text{Hz}$ ]	$A_{\text{WIRE}}$ [mmag]	$\phi_{\text{WIRE}}$ [0..1]	$A_B$ [mmag]	$\phi_B$ [0..1]
$f_1$	2442.0566(2)	0.652(5)	0.506(2)	1.54(3)	0.490(3)
$f_2$	2265.43(2)	—	—	—	—
$f_3$	2341.79(1)	—	—	—	—
$f_4$	2366.47(4)	0.047(8)	0.67(4)	—	—
$f_5$	2566.98(3)	0.044(7)	0.18(3)	—	—
$f_6$	2411.8822(9)	0.149(5)	0.471(6)	0.28(3)	0.46(2)
$f_7$	2472.2272(5)	0.188(5)	0.041(4)	0.42(3)	0.06(2)
$f_1^-$	2439.47(2)	0.089(5)	0.06(1)	—	—
$f_1^+$	2444.64(2)	0.079(5)	0.97(2)	—	—

Notes:  $f_2$  and  $f_3$  were detected by Kurtz et al. (1994), but are not present in the *WIRE* data.  $f_5$  was only detected in the Jul'06 data.  $f_1^+$  and  $f_1^-$  correspond to  $f_1 \pm f_{\text{rot}}$ , where  $f_{\text{rot}}$  is the rotational frequency.

(2005) reanalysed sparse data collected from the literature spanning 14 y and showed a rotation curve consistent with  $P_{\text{rot}} = 4.4794 \text{ d}$ . We have repeated that exercise including a new measurement (Hubrig et al. 2004), making the time span 23 y, and find a marginal indication of magnetic variability with the known rotation period  $P_{\text{rot}} = 4.4794 \text{ d}$ , at the  $2.5\sigma$  significance level, if we neglect one outlying positive field measurement. This does not give us confidence that magnetic variability with the rotation period has actually been detected, and it is certainly not possible to give a time of magnetic maximum that can be compared to the time of rotational light minimum, or to the time of pulsation maximum.

We can conclude that the longitudinal field for  $\alpha$  Cir has been detected. The mean value derived from the data of Hubrig et al. (2004) is the most reliable at  $-239 \pm 27 \text{ G}$  (internal error). The evidence from the data in the literature is that the longitudinal field is probably not reversing; i.e. only one magnetic pole is seen over the rotation period, implying that  $i + \beta < 90^{\circ}$ , where  $i$  is the rotational inclination and  $\beta$  is the magnetic obliquity of the negative pole. For oblique magnetic rotators, the strength of the measured longitudinal magnetic field is proportional to  $\cos \alpha$ , where  $\alpha$  is the angle between the magnetic pole and the line-of-sight. That varies as

$$\cos \alpha = \cos i \cos \beta + \sin i \sin \beta \cos \Omega t, \quad (1)$$

where  $\Omega$  is the rotational frequency.

Our rotational phase zero – the time of rotational light minimum in Fig. 2 – is therefore the time when the largest of the two equatorial spots is on the observed hemisphere closest to the line-of-sight. Since two equatorial spots are needed to describe the light curve, they cannot be associated with the one magnetic pole that is always visible. The pulsation pole is also not associated with the spots, as we will see in Sect. 4. This is not normal for an roAp star, hence for all interpretation related to the rotational light curve, we proceed with caution.

### 3.2 Analysis of the rapid oscillations

We analysed the rapid oscillations in the *WIRE* and SAO light curves using the Fourier analysis package PERIOD04

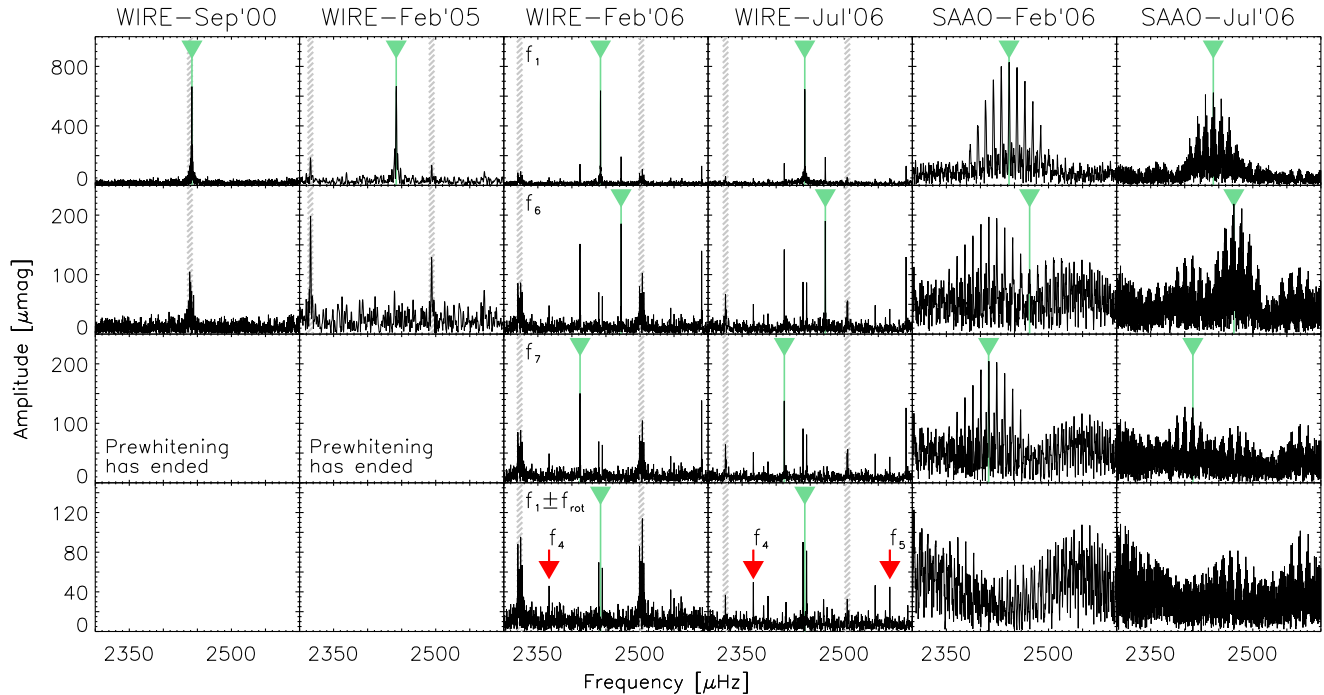


**Figure 3.** Prewhitening of the *WIRE* and *SAAO* data sets. In each row the triangles and vertical lines mark the frequency being subtracted and the hatched grey regions mark the harmonics of the *WIRE* orbit. In the amplitude spectra from 2000 and 2005 we detect only the dominant  $f_1$  mode. All four amplitude spectra from 2006 show  $f_1$ ,  $f_6$  and  $f_7$ , although for the *SAAO* data the S/N is poor for the two weaker modes. In the bottom row four additional peaks,  $f_1 \pm f_{\text{rot}}$ ,  $f_4$ , and  $f_5$ , are marked in the *WIRE* data sets from 2006.

(Lenz & Breger 2005) and a Discrete Fourier Transform (Kurtz 1985), and we found excellent agreement between the two methods. We first subtracted the rotation signal, as found above. We initially analysed each data set independently, and the prewhitening process is shown in Fig. 3. The *top panels* show the amplitude spectra of the six observed light curves, i.e. four from *WIRE* and two from *SAAO*. In each row of panels the frequency with the highest amplitude is marked by the triangle and a vertical line. The hatched regions mark the harmonics of the orbital frequency of *WIRE*, which changed considerably from Sep'00 ( $f_{\text{WIRE}} = 174.2 \mu\text{Hz}$ ) to Jul'06 ( $f_{\text{WIRE}} = 178.9 \mu\text{Hz}$ ) due to the decay of the orbit. The signal seen at the orbital harmonics ( $n \times f_{\text{WIRE}}$ ) has leaked from drift noise at low frequencies. Note that in the Sep'00 spectrum, the main  $f_1$  mode lies close to an orbital harmonic ( $n = 14$ ). The second row of panels in Fig. 3 shows the residual amplitude spectra after subtracting the  $f_1$  mode at  $2442 \mu\text{Hz}$ . No additional significant peaks are detected in the *WIRE* data from Sep'00 and Feb'05. However, both the *WIRE* data sets from 2006 and the simultaneous *SAAO* data show two peaks,  $f_6$  and  $f_7$ , that have not been detected in previous campaigns. Interestingly, these peaks lie symmetrically at  $\pm 30 \mu\text{Hz}$  around the main mode. Note that in the amplitude spectra from *SAAO*, the  $1 \text{ c d}^{-1}$  alias peaks are sometimes slightly higher than the “true peak” (known from the *WIRE* data and marked by the vertical line). This problem is well known for single-site data, especially at low S/N. Fortunately, there is no ambiguity in our case since we have the high-S/N satellite data. In the *bottom panels* in Fig. 3 we see no signal above the noise in either of the *SAAO* data sets. In the Feb'06 and Jul'06 *WIRE* data sets we detect

additional peaks<sup>1</sup> at  $f_1^\pm = f_1 \pm f_{\text{rot}}$  and  $f_4 = 2366 \mu\text{Hz}$ , while in Jul'06 we detect also a low amplitude peak at  $f_5 = 2566 \mu\text{Hz}$ .

### 3.3 Combining the 2006 *WIRE* data sets

Since the two *WIRE* data sets from 2006 contain nearly the same peaks in the amplitude spectrum, we combined the data sets to be able to extract more precise frequencies: the formal error on frequency scales with  $1/T_{\text{obs}}$ , where  $T_{\text{obs}}$  is the baseline of the observations (e.g. Montgomery & O'Donoghue 1999). There is a caveat when combining these data due to the 4-month gap between them, resulting in a spectral window with many sub-peaks that have almost equal amplitude. To illustrate the problem, spectral windows are shown in Fig. 4 for the Feb'06 data set and the combined Feb'06 + Jul'06 data sets. In the *top panel* the detected frequencies are marked by arrows, including  $f_2$  and  $f_3$ , which were observed by Kurtz et al. (1994) but are not present in the *WIRE* data sets.

To see if there is any ambiguity when extracting the frequencies, we repeated the analysis for 100 simulations of the combined Feb'06 + Jul'06 time series, to see how often the input frequencies were correctly identified. To make the simulations, we followed the approach of Bruntt et al. (2007, their Appendix B). The simulations include the observed frequencies, the rotational double wave, white noise, and a  $1/f$  noise component consistent with the observations. The simulations were analysed by an automatic prewhitening procedure. The inserted frequencies were retrieved in all 100 cases, except 11/100 for  $f_4$  and 3/100 for  $f_1^\pm$  (these modes have  $S/N \sim 6$  and 10). In these cases frequencies offset by  $\pm 0.083 \mu\text{Hz}$

<sup>1</sup>  $f_{\text{rot}} = 1/P_{\text{rot}} = 2.5841 \pm 0.0001 \mu\text{Hz}$ .

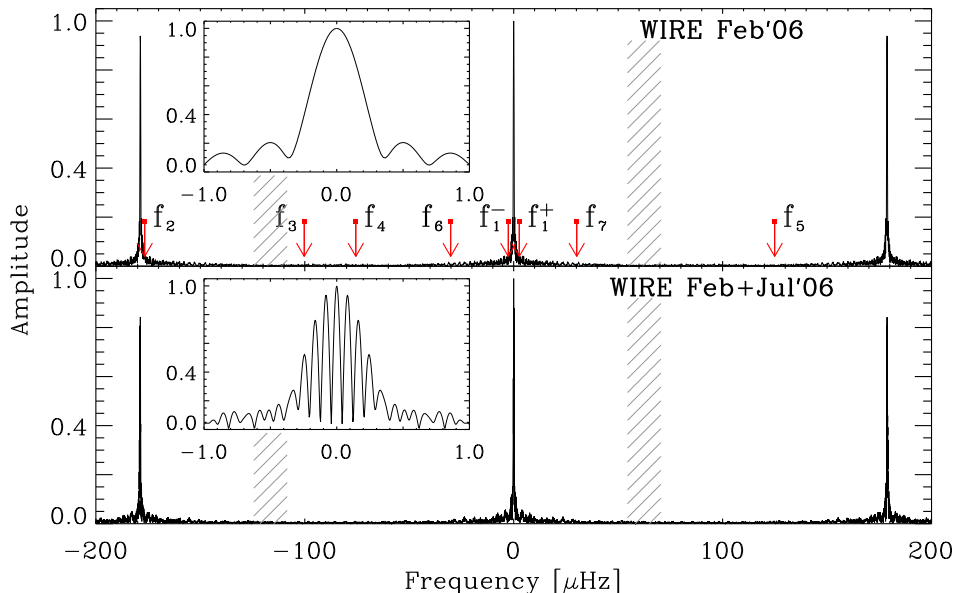


**Figure 4.** Spectral windows for the Feb'06 data set (*top panel*) and the combined Feb'06 + Jul'06 data sets (*bottom panel*) from *WIRE*. The insets show details of the central peak. The arrows mark the positions of the frequencies detected in  $\alpha$  Cir and the hatched regions mark the location of the orbital harmonics. Note that  $f_2$  (close to an alias peak of  $f_1$ ) and  $f_3$  are from Kurtz et al. (1994) and were not detected in the *WIRE* data sets.

were picked by the automatic procedure, corresponding to an alias peak offset by  $\pm 1/T_{\text{gap}}$ , where  $T_{\text{gap}}$  is the duration of the gap. Due to these relatively high false-alarm ratios, we will quote results for the low amplitude modes using only the best data set from Jul'06.

In Table 3 we give the final results for the combined data set for  $f_1$ ,  $f_6$  and  $f_7$ , while the results for the other modes are based on the Jul'06 data set. Note that the frequencies  $f_1^\pm$  were fixed, with  $f_1$  from the combined data set and  $f_{\text{rot}} = 1/P_{\text{rot}}$  from Sect. 3.1. We used the results of the simulations to determine the uncertainties of the frequency, amplitude, and phase calculated as the standard deviation of the extracted parameters. The uncertainties are given in the parentheses in Table 3, and are in general agreement with theoretical expressions, assuming pure white noise (e.g. Montgomery & O'Donoghue 1999).

### 3.4 Calibration of the *WIRE* photometry

To calibrate the measured amplitude and phases of the *WIRE* photometry, we analysed the combined ground-based Johnson *B* data from the two SAAO runs, obtained at the same time as the two *WIRE* data sets from 2006. We made simulations of the data as described in Sect 3.3, which showed that the automatic prewhitening was seriously affected by the complicated spectral window with strong  $1 \text{ c d}^{-1}$  alias peaks. Fortunately, the frequencies of  $f_1$ ,  $f_6$  and  $f_7$  are determined very accurately from the *WIRE* data and we therefore held the frequencies fixed when determining their amplitudes and phases. The fitted values are listed in the last two columns in Table 3.

We measured the amplitude ratio and the phase shift between the *WIRE* and SAAO observations. The amplitude ratios for the three modes  $f_1$ ,  $f_6$  and  $f_7$  are:  $A_B/A_{\text{WIRE}} = 2.36 \pm 0.11$ ,  $1.88 \pm 0.38$ , and  $2.23 \pm 0.36$ , with a weighted mean  $\langle A_B/A_{\text{WIRE}} \rangle = 2.32 \pm 0.10$ . The results for the  $f_1$  mode shows a small but significant phase shift of  $\phi_{\text{WIRE}} - \phi_B = +5.8 \pm 1.3$ . The phases of

$f_6$  and  $f_7$  are in agreement with this shift, but the uncertainties are three times larger and cannot be used to constrain the phase shift.

Kurtz & Balona (1984) made simultaneous observations in Johnson *B* and *V* and measured only small phase shifts  $\phi_V - \phi_{B-V} = +13^\circ \pm 6^\circ$  and  $\phi_V - \phi_B = -7.4 \pm 5.1$ . They measured the amplitude ratio for  $f_1$  to be  $A_B/A_V = 2.28 \pm 0.26$ , which is essentially the same as our ratio of  $A_B/A_{\text{WIRE}}$ . Thus the amplitude in the *WIRE* data is similar to that which would be observed through a Johnson *V* filter, strongly suggesting that the bandpass of the *WIRE* photometry is centered at about the same wavelength as Johnson *V*. The interpretation of the small phase shifts is more problematic, since it is well-known from high resolution spectroscopic studies that the pulsation phase in roAp stars can be a sensitive function of atmospheric depth of the observations (see, e.g., Kurtz et al. 2006a, Ryabchikova et al. 2007).

## 4 IDENTIFICATION OF THE PRIMARY MODE

In the following we will discuss the possible mode identification of the primary  $f_1$  mode using the relative amplitudes of the rotational sidelobes. This is done in the framework of the oblique pulsator model, which postulates that the axis of the non-radial pulsation modes is inclined to the rotation axis of the star. In some versions of the model the pulsation axis coincides with the magnetic axis (Kurtz 1982, Shibahashi 1986, Kurtz & Shibahashi 1986, Shibahashi & Takata 1993, Takata & Shibahashi 1995), while in another version the pulsational axis may be inclined to both the rotational and magnetic axes (Bigot & Dziembowski 2002). Here, we interpret the rotational frequency triplet  $f_1 \pm f_{\text{rot}}$  in terms of the formalism of Shibahashi (1986) and Kurtz & Shibahashi (1986).

We expect the observed modes in photometry to be of low degree (typically  $l \leq 2$ ), given that generally perturbations associated with modes of higher degree cancel out when averaged over the stellar disk. However, this may not always be the case in roAp

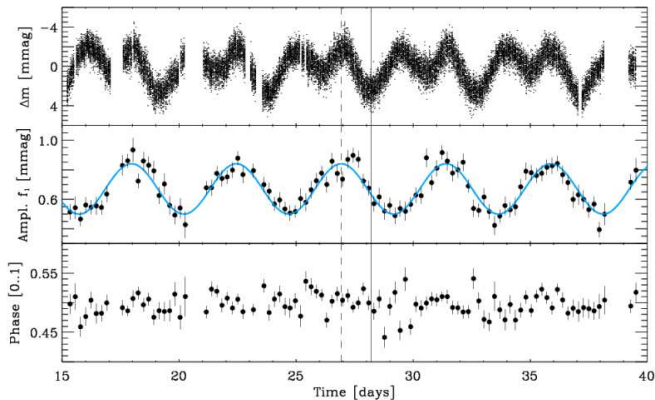


**Figure 5.** The *top panel* is the light curve of  $\alpha$  Cir from *WIRE* in Jul’06. The *middle* and *bottom panel* shows variation of the amplitude and phase of the primary mode at  $2442 \mu\text{Hz}$  determined by fits to subsets of the light curve. The vertical lines mark the time zero points at maximum amplitude ( $t_{\text{max}}$ ; dashed line) and minimum light ( $t_{\text{rot}}$ ; solid line).

stars, since the presence of strong magnetic fields that permeate the surface of these stars may result in a distortion of the eigenfunctions at the surface (Dziembowski & Goode 1996; Cunha & Gough 2000; Saio & Gautschy 2004). Thus, a mode of degree higher than  $l = 2$  could in principle give rise to lower-degree components at the surface and still be detected. If the magnetic perturbations are symmetric about the magnetic equator, as is the case for pure dipolar or pure quadrupolar magnetic topologies, the additional components of the perturbed eigenfunctions will have the same parity (odd or even  $l$ ) as the non-perturbed one. We will discuss this further in the third paper of this series (Brandão et al., in preparation), in which detailed magnetic modelling of the pulsations in  $\alpha$  Cir will also be presented.

#### 4.1 Properties of the rotational sidelobes

We observed two frequency sidelobes around the principal pulsation frequency  $f_1$ , separated by  $2.58 \mu\text{Hz}$ , which is the same as the rotational frequency. In the two amplitude spectra from *WIRE* 2006 in Fig. 3 the sidelobes at  $f_1 \pm f_{\text{rot}}$  are clearly seen. To measure the amplitudes and phases of the sidelobes we assume they are separated by exactly the rotation frequency, as required by the oblique pulsator model. We use the highest precision value we have for the rotational frequency (cf. Sect. 3.1;  $f_{\text{rot}} = 2.5841 \pm 0.0001 \mu\text{Hz}$ ) and fitted an equally spaced frequency triplet about  $f_1 = 2442.0566 \mu\text{Hz}$  by least squares, with the requirement that the zero point of the time scale be chosen such that the phases of the rotational sidelobes be equal (i.e.  $\phi_1^+ = \phi_1^-$ ), as expected for axisymmetric modes in the oblique pulsator model (Kurtz 1982).

The results of that fit are shown in Table 4 for the zero point in time  $t_{\text{max}} = \text{HJD}245\,3935.91562$ . The amplitudes of the two rotational sidelobes are equal to within  $1.5\sigma$ , i.e.  $A_1^+/A_1^- = 0.854 \pm 0.096$ . This is consistent with the magnetic perturbations to the eigenfrequencies being very much stronger than the rotational perturbations. The zero point in time for the least-squares fit was chosen such that the phases of the rotational sidelobes are equal, but the phase of the central frequency of the triplet was not constrained by this choice of  $t_{\text{max}}$ . The nearly identical phases (they differ by  $1.6\sigma$ ) are thus consistent with a purely geometrical am-

**Table 4.** A least squares fit to all of the *WIRE* 2006 data of the principal frequency,  $f_1 = 2442.0566 \mu\text{Hz}$  and its two rotational sidelobes which – within the oblique pulsator model – are separated by exactly the rotation frequency of  $f_{\text{rot}} = 2.5841 \pm 0.0001 \mu\text{Hz}$ .

ID	$f$ $\mu\text{Hz}$	$A$ mmag	$\phi$ [0..1]
$f_1^-$	2439.4725	$0.082 \pm 0.006$	$0.423 \pm 0.011$
$f_1$	2442.0566	$0.618 \pm 0.006$	$0.4050 \pm 0.0014$
$f_1^+$	2444.6407	$0.070 \pm 0.006$	$0.423 \pm 0.013$

plitude modulation with rotational aspect in the oblique pulsator model.

To investigate the variation of the amplitude we followed the approach of Kurtz et al. (1994) to analyse the *WIRE* Jul’06 data set, which has the highest S/N of all of our data. We first subtracted the other modes from the data set, i.e. the rotational double wave  $f_A + f_B$  (Sect. 3.1) and the low amplitude modes  $f_4 - f_7$  (Sect. 3.2). We then split the data into subsets containing 30 pulsation cycles of  $f_1$ , corresponding to time bins of  $\Delta t \simeq 3.4$  h. In each subset we found the amplitude and phase of the  $f_1$  mode by least squares, holding the frequency fixed. We find that the amplitude of  $f_1$  is modulated by the rotation while the phase is not. The result is shown in Fig. 5, where the variations in amplitude and phase of  $f_1$  are shown in the middle and bottom panels, respectively. The top panel shows the *WIRE* light curve for comparison. The time of minimum light ( $t_{\text{rot}}$ , as defined in Sect. 3.1) is marked with a solid line and the time of maximum amplitude ( $t_{\text{max}}$ ) is marked with a dashed line. The delay in the maximum amplitude with respect to the zero point for the rotation phase (Sect. 3.1) is  $\Delta\phi = \phi_{\text{max}} - \phi_{\text{rot}} = 0.287 \pm 0.003$ . In other words, the time of maximum amplitude occurs at rotation phase  $1 - \Delta\phi = 0.713$  (see Fig. 2). Comparison of the time zero points for the rotational light variation and the pulsation maximum gives nearly the same result: the rotational phase is  $\phi_{\text{rot}} = (t_{\text{max}} - t_{\text{rot}})/P_{\text{rot}} = -0.289 = 0.711$ .

For an axisymmetric dipole mode ( $l = 1, m = 0$ ) aligned with the magnetic field, and for spots centred on the magnetic poles, we expect the time of pulsation maximum to coincide with the time of rotational light minimum, whereas, as can be seen in Fig. 5, rotational phase 0.71 coincides with one of the rotational light maxima. The essentially pure amplitude modulation with a sinusoidal variation over the rotation cycle is consistent with a pure dipole pulsation mode, leading to the conclusion that the spots are not concentric with the magnetic field. While small departures between the spots and magnetic poles do occur in some magnetic Ap stars, e.g. in the roAp star HR 3831 (Kurtz et al. 1992), the case of  $\alpha$  Cir requires equatorial spots far from the pulsation pole. For further progress, new, very precise measurements of the magnetic field of  $\alpha$  Cir are needed to show a convincing rotational variation, as we pointed out in Sect. 3.1.

#### 4.2 Is $f_1$ a dipole or a quadrupole mode?

The observed pulsation amplitude of an obliquely pulsating non-radial mode varies with rotation, as the aspect of the mode changes. This gives rise to a frequency multiplet, separated by the rotation frequency, that describes the amplitude modulation (and also phase modulation, if present). Within the formalism of the oblique pulsator model (Shibahashi 1986; Kurtz & Shibahashi 1986; Kurtz et al. 1990) we have calculated the rotational am-

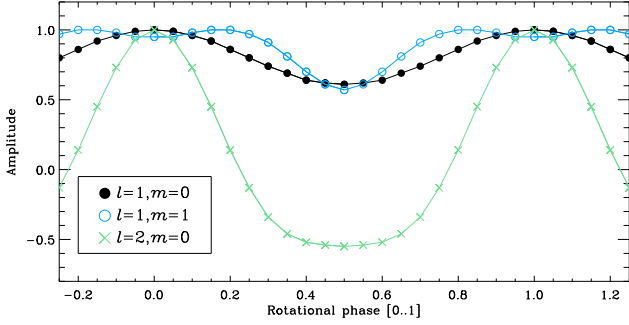


**Figure 6.** The relative amplitude modulation over the rotation cycle for two dipole modes,  $l = 1, m = 0$  (solid circles) for  $\beta = 18^\circ$  and  $l = 1, m = 1$  (open circles) for  $\beta = 108^\circ$ , and the axisymmetric quadrupole mode with  $l = 2, m = 0$  (crosses) for  $\beta = 51^\circ$  (in all cases  $i = 37^\circ$ ). The values of  $\beta$  have been derived from the constraints of the amplitude ratio of the rotationally split frequency triplet to the amplitude of the principal frequency as described in detail in the text. For each mode the maximum amplitude has been normalised to 1.

plitude modulation expected for three possible pulsation modes, ( $l = 1, m = 0$ ), ( $l = 1, m = \pm 1$ ), and ( $l = 2, m = 0$ ), such that the amplitude modulation agrees with the observed amplitudes of the rotationally split frequency triplet given in Table 4. The results are shown in Fig. 6 and each case will be discussed in detail below.

#### 4.2.1 An axisymmetric dipole mode ( $l = 1, m = 0$ )

Whatever the relationship between the rotational light curve and the pulsation, the frequency triplet of Table 4 is consistent with an axisymmetric dipole mode, or any mode of higher degree to which distortion by the magnetic field could result in the addition of a significant ( $l = 1, m = 0$ ) component. This leads to the constraint (Kurtz et al. 1990):

$$\frac{A_{+1} + A_{-1}}{A_0} = \tan i \tan \beta = 0.246 \pm 0.014 = r_1, \quad (2)$$

where  $i$  is the rotational inclination and  $\beta$  is the magnetic obliquity of the negative pole, and  $A_{+1}$ ,  $A_{-1}$  and  $A_0$  refer to the amplitudes of the rotational sidelobes and the principal frequency. Since we have already determined the rotational inclination to be  $i = 37 \pm 4^\circ$  in Sect. 3.1, that leads to  $\beta = 18 \pm 3^\circ$ . These values are consistent with only one magnetic pole being visible over the rotation cycle, i.e. with  $i + \beta < 90^\circ$  as we have discussed in Sect. 3.1. Fig. 6 shows an axisymmetric dipole mode with these values of  $\beta$  and  $i$  (solid circles). It has a sinusoidal amplitude modulation, which is in agreement with the observed modulation in Fig. 5.

The oblique rotator model for a dipole magnetic field leads to a similar constraint on the geometry; Hubrig et al. (2007) found  $\tan i \tan \beta = 0.66$  with no estimated error. We cannot, therefore, assess whether there is an inconsistency between these derivations of  $\tan i \tan \beta$ , but note that Hubrig et al. (2007) find  $i = 38^\circ$ ,  $\beta = 40^\circ$ , hence  $i + \beta < 90^\circ$ , also indicating that only one magnetic pole is visible.

#### 4.2.2 A non-axisymmetric dipole mode ( $l = 1, m = \pm 1$ )

Non-axisymmetric dipole modes ( $l = 1, m = \pm 1$ ) within the oblique pulsator model constraints on the geometry (Kurtz & Shibahashi 1986, Shibahashi 1986) give

$$\frac{A_{+1} + A_{-1}}{A_0} = -\frac{\tan i}{\tan \beta} = r_1, \quad (3)$$

which leads to  $\beta = 108 \pm 3^\circ$  for  $i = 37 \pm 4^\circ$ . This implies that both magnetic poles should be observed, contrary to observations. The amplitude modulation of a sectoral  $l = 1, m = 1$  mode with these values of  $\beta$  and  $i$  is shown in Fig. 6 (open circles) and exhibit a double wave that is not observed; this is because both poles are seen, but from different aspect. The pulsation mode can therefore not be a dipole mode with  $m = \pm 1$ .

#### 4.2.3 An axisymmetric quadrupole mode $l = 2, m = 0$

From our theoretical modelling in Sect. 5.1 we show that both even and odd  $l$  modes are present, so it is worth exploring whether the principal mode could have even degree, seen by the observer as a quadrupole mode. For an axisymmetric quadrupole mode with  $l = 2, m = 0$  we expect a frequency quintuplet with separations of  $f_{\text{rot}} = 2.5841 \mu\text{Hz}$ . Since the outer two frequencies of this quintuplet are not observed, we assume that their amplitudes are below the  $3\sigma$  detection limit (i.e.  $A_{\pm 2} < 0.018 \pm 0.002$  mmag) and solve for the magnetic obliquity that is consistent with this. We then expect (Kurtz et al. 1990; Shibahashi 1986)

$$\frac{A_{+1} + A_{-1}}{A_0} = \frac{12 \sin \beta \cos \beta \sin i \cos i}{(3 \cos^2 \beta - 1)(3 \cos^2 i - 1)} = r_1, \quad (4)$$

and

$$r_2 \equiv \frac{A_{+2} + A_{-2}}{A_0} \quad (5)$$

$$= \frac{3 \sin^2 \beta \sin^2 i}{(3 \cos^2 \beta - 1)(3 \cos^2 i - 1)} \quad (6)$$

$$\leq 0.058 \pm 0.005. \quad (7)$$

We can divide Eq. (6) by Eq. (4) to yield

$$\tan i \tan \beta = \frac{4r_2}{r_1} \leq 0.94 \pm 0.10. \quad (8)$$

For  $i = 37 \pm 4^\circ$ , Eq. (8) yields  $\beta = 51 \pm 5^\circ$ . This also fulfills the requirement that  $i + \beta < 90^\circ$ , but the amplitude variation is clearly not sinusoidal with rotation, as can be seen in Fig. 6 (cross symbols). In fact, for this quadrupole the amplitude goes through zero and reverses phase over the rotation cycle, in clear conflict with the observations. We therefore conclude that the principal frequency does not have the observational properties of an axisymmetric quadrupole mode.

### 4.3 Concluding remarks on the mode identification of $f_1$

The apparent lack of any rotational phase variation (Sect. 4.1) and the rotational amplitude variation of the principal pulsation mode (Sect. 4.2) strongly support the supposition that the principal mode has the observational properties of an axisymmetric  $l = 1, m = 0$  dipole mode. Note well, however, that we do not constrain our theoretical modelling in the next section to dipole modes for the principal pulsation mode, since magnetic perturbations may make modes of a different degree appear to be very similar to dipole modes observationally.

## 5 ASTEROSEISMOLOGY OF $\alpha$ Cir

In the following we will compare theoretical pulsation models with the new observational constraints consisting of the improved fun-

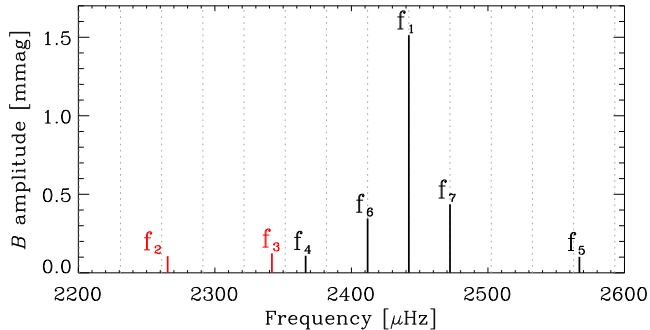


**Figure 7.** Frequencies detected in  $\alpha$  Cir from the *WIRE* data and  $f_2/f_3$  from Kurtz et al. (1994). The vertical dashed lines mark the mean separation between  $f_6$ ,  $f_1$  and  $f_7$ .

damental parameters (Paper I) and the detection of the large separation in the current work.

Before comparing the observed and theoretical frequencies it is crucial to include only the observed frequencies for which there are no ambiguities about their detection. In Fig. 7 we show a schematic frequency spectrum of seven modes that we believe are due to pulsation and intrinsic to  $\alpha$  Cir. In our list of secure frequencies in Table 3 we have included the five frequencies  $f_1$ – $f_5$  detected by Kurtz et al. (1994) and the two new frequencies  $f_6$  and  $f_7$ . In Fig. 7 we have scaled the amplitudes to the  $B$  filter system using the ratio  $A_B/A_{WIRE}$  from Sect. 3.4, and for  $f_2$  and  $f_3$  we use the scaling  $A_v/A_B = 1.29$  (Kurtz et al. 1994). The vertical dashed lines correspond to the average separation between consecutive modes in the triplet  $f_6 + f_1 + f_7$ .

The frequencies  $f_2$  and  $f_3$  were not detected in our data although from the observed noise level in the *WIRE* 2006 data and the observed amplitude we should have detected them with a S/N ratio around 6–8. A likely explanation is that their amplitudes have changed over time. Alternatively, it is possible that  $f_2$  was not detected due to its proximity to the sideband  $f_2 \simeq f_1 - f_{WIRE}$  ( $\Delta f = 2.3 \mu\text{Hz}$ ), while the detection of  $f_3$  was perhaps not possible due to it being relatively close to an orbital harmonic ( $n = 13$ ,  $\Delta f = 16.2 \mu\text{Hz}$ ). These possibilities are illustrated in Fig. 4.

The frequencies  $f_6$  and  $f_7$  must have appeared some time between Feb’05 and Feb’06, since they were not detected in the *WIRE* data sets from Sep’00 and Feb’05. If their amplitudes had not changed, the peaks should have been detected, with S/N of about 14 and 7 in the amplitude spectra from Sep’00 and Feb’05, respectively. Nevertheless, as they are seen in both of the simultaneous runs with *WIRE* and from SAAO in 2006, they must be intrinsic to  $\alpha$  Cir.

A few additional frequencies have been reported based on spectroscopic campaigns (Balona & Laney 2003; Kurtz et al. 2006b), but we have not included them in the modelling. The frequencies reported by Balona & Laney (2003) are clearly affected by  $1 \text{ c d}^{-1}$  aliasing problems, and the data analysis by Kurtz et al. (2006b) is complicated by the relatively poor frequency resolution while at the same time the frequencies lie close to the principal mode.

The frequencies shown in Fig. 7 contain information about the average properties of  $\alpha$  Cir as well as details about its internal structure and magnetic field. In the following we will attempt a forward comparison with the theoretical oscillation spectra obtained from models. To avoid confusion with the observed frequencies  $f$ , we

shall designate the theoretical frequencies by  $\nu_{n,l}$ , where  $n$  and  $l$  are, respectively, the radial order and the degree of the eigenmodes.

## 5.1 The large separation

The most commonly used observable quantity when studying high-overtone p mode oscillations in stars is the large frequency separation  $\Delta\nu_{n,l}$ , defined as the difference between modes of the same degree and consecutive radial orders:  $\Delta\nu_{n,l} \equiv \nu_{n+1,l} - \nu_{n,l}$ . The large separation is a function of frequency, but for high radial orders the dependence is small. In fact, in a spherically symmetric star, the frequencies of linear adiabatic acoustic pulsations of high radial order are expected to follow the asymptotic relation (Tassoul 1980):

$$\nu_{n,l} \simeq \Delta\nu_0 (n + l/2 + 1/4 + \alpha) + \epsilon_{n,l}, \quad (9)$$

where  $\Delta\nu_0 = (2 \int_0^R dr/c)^{-1}$ ,  $R$  is the stellar radius,  $c$  is the sound speed and  $r$  is the radial coordinate. The value of  $\alpha$  depends on the properties of the reflection layer near the surface, and  $\epsilon_{n,l}$  is a small term that depends mostly on the conditions in the stellar core. It can be seen that  $\Delta\nu_0$  is the inverse of the sound travel time across the diameter of the star.

The high frequency of the oscillations observed in  $\alpha$  Cir indicates that these are indeed acoustic oscillations with high radial order. Thus one may expect to find in the oscillation spectrum a regular pattern corresponding to the asymptotic relation. However, the asymptotic analysis assumes spherical symmetry of the star. In  $\alpha$  Cir, as in other roAp stars, the presence of a strong magnetic field introduces a source of deviation from spherical symmetry that can shift the oscillation frequencies significantly from the asymptotic values (Cunha & Gough 2000; Cunha 2006; Saio & Gautschy 2004). According to these studies, one may expect to still see regular frequency spacings in some parts of the oscillation spectra, but abnormal spacing might also be found as in the well-studied case of HR 1217 (Kurtz et al. 2005; Cunha 2001).

The observed frequencies  $f_6$  and  $f_7$  lie almost equidistantly around  $f_1$ , to within a few nHz:  $f_1 - f_6 = 30.1746 \pm 0.0009 \mu\text{Hz}$  and  $f_7 - f_1 = 30.1707 \pm 0.0005 \mu\text{Hz}$ . We determine the average separation from the slope of a first order polynomial fitted to the three frequencies:  $\Delta f_{\text{obs}} = 30.173 \pm 0.004 \mu\text{Hz}$ . To be conservative we adopt the difference between the two values as the uncertainty. This separation is marked by the vertical dashed lines in Fig. 7. We note that the frequencies  $f_2$  and  $f_5$  appear to roughly agree with the spacing.

If the regular frequency spacing of  $f_6 + f_1 + f_7$  involves modes with degrees of different parity, and if their frequencies are not significantly modified by the magnetic field, then we may conclude that the large separation is  $\Delta\nu_0 \approx 2\Delta f_{\text{obs}}$ . Otherwise, if only modes with degrees of the same parity are present, we have  $\Delta\nu_0 \approx \Delta f_{\text{obs}}$ . Since  $\Delta\nu_0$  depends essentially on the mean density of the star, these two possibilities correspond to stars with very different mean densities. It is straightforward to determine, based on non-asteroseismic observables of  $\alpha$  Cir, which one of these possibilities is more plausible.

## 5.2 The pulsation model

To compute theoretical pulsation frequencies we first calculated a reference equilibrium model of  $\alpha$  Cir using the stellar evolution

**Table 5.** Global parameters of the CESAM model used to represent  $\alpha$  Cir. As input parameters we used  $X_0 = 0.70$ ,  $Y_0 = 0.28$ ,  $\alpha = 1.6$  and no overshooting.  $X_0$  and  $Y_0$  are, respectively, the initial hydrogen and helium abundances and  $\alpha$  is the mixing length parameter. The mass,  $M$ , luminosity,  $L$ , and radius,  $R$ , are expressed in solar units.  $C_\nu$  is the homologous constant defined in Eq. (10).

$M/M_\odot$	$L/L_\odot$	$T_{\text{eff}}$ [K]	$R/R_\odot$	$C_\nu$ [ $\mu\text{Hz}$ ]
1.715	1.019	7421	1.96	130.8

code CESAM<sup>2</sup> (Morel 1997). The fundamental parameters used for this model are given in Table 5 and are adopted from our analysis of interferometric data and spectra calibrated in flux as described in Paper I. The position corresponding to these parameters is given by the asterisk in the Hertzsprung-Russell (HR) diagram in Fig. 8.

To calculate the theoretical oscillation frequencies for this model we used the linear adiabatic oscillation code ADIPLS (Christensen-Dalsgaard 2008). Since the observed frequencies are above the acoustic cutoff frequency for the reference model, we have applied at the outermost point of the pulsation models a fully reflective boundary condition of the type  $\delta p = 0$ , where  $\delta p$  is the Lagrangian perturbation to the pressure. The physical mechanism responsible for the reflection of the oscillations in roAp stars has been under debate for decades. It is likely that the reflection of the oscillations results from the direct effect of the magnetic field (Sousa & Cunha 2008). Despite the small value of the longitudinal magnetic field of  $\alpha$  Cir (Hubrig et al. 2004; cf. Sec. 3.1), we note that the magnetic field intensity of this star is not necessarily small. If we assume a dipolar topology and the magnetic obliquity and rotational inclination derived in Sect. 4.2.1, we find a polar magnetic strength of  $\sim 1$  kG. Moreover, if the magnetic field has a quadrupolar component, its polar intensity will be even stronger. A comparison between magnetic and gas pressures in the outer layers of a magnetic stellar model with parameters similar to  $\alpha$  Cir was presented by Cunha (2007). From their discussion it is clear that even a 1 kG magnetic field has a strong effect on the dynamics of the oscillations throughout the whole atmosphere of a typical roAp star. Thus, it is expected that through mode conversion part of the mode energy is passed onto magnetic waves in the atmosphere. The energy transferred to these magnetic waves is kept in the mode. Thus, if the energy input in each cycle through the excitation mechanism (Balmforth et al. 2001; Cunha 2002; Saio 2005) is enough to compensate for the fraction of the mode energy that is lost through running acoustic waves in the atmosphere (Sousa & Cunha 2008) and through running magnetic waves in the interior (Roberts & Soward 1983), the mode will be over-stable and may reach a detectable amplitude.

The use of a fully reflective boundary condition is an artificial way to induce reflection of pulsations in the theoretical model and may shift the computed frequencies of individual modes away from their true values (Cunha 2006). Nevertheless, its effect on the individual mode frequencies is expected to be systematic and, thus, should cancel out when computing pulsating quantities that are based on frequency differences, particularly when these differences involve only modes of the same degree. Since this is indeed the case for the large separation, our computed values will not be significantly affected by the adopted boundary condition.

<sup>2</sup> The CESAM code is available at <http://www.astro.up.pt/corot/models/cesam/>

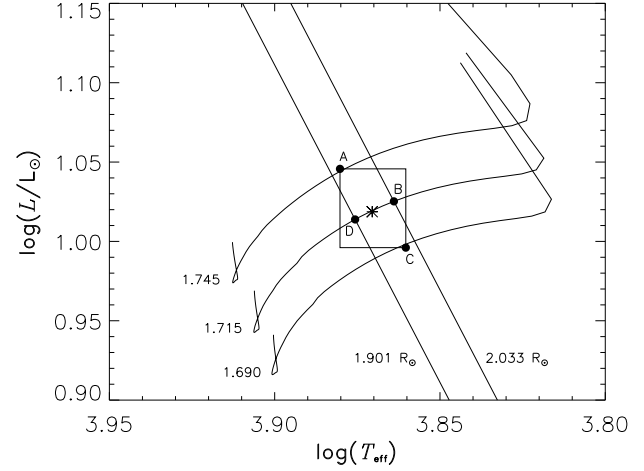


**Figure 8.** H-R diagram with three evolution tracks from CESAM. The position of our reference model is marked with an asterisk and four additional models considered in our analysis are labeled A, B, C and D. The rectangle marks the  $1\sigma$  uncertainty on  $T_{\text{eff}}$  and  $L/L_\odot$  and the two diagonal lines correspond to constant radii consistent with the  $1\sigma$  uncertainty on the interferometric measurements from Paper I.

The average large separation of the reference model is  $\langle \Delta\nu_{n,l} \rangle = 62.5 \mu\text{Hz}$ . Modes of degrees  $l = 0, 1, 2$  and  $3$ , with frequencies around the observed values, were used to calculate this average. This value is close to  $2\Delta f_{\text{obs}}$  and so the solution  $\Delta\nu_0 \approx \Delta f_{\text{obs}}$  is firmly rejected. This means that modes with degrees of alternating parity must be involved in the regular frequency pattern observed in the triplet  $f_6, f_1, f_7$ .

It is beyond the scope of the present work to make a detailed model of  $\alpha$  Cir. However, it is worth inspecting how the results for our model compare with those for similar models placed within the region of uncertainty associated with the global parameters of  $\alpha$  Cir. We have considered four additional models, labeled A, B, C and D in Fig. 8. These models lie at the extremes of the  $1\sigma$ -uncertainty rectangle ( $T_{\text{eff}} = 7420 \pm 170$  K,  $L/L_\odot = 10.51 \pm 0.60$ ) and inside the strip defined by the two lines of constant radius corresponding to  $R/R_\odot = 1.967 \pm 0.066$  (the interferometric radius from Paper I). To estimate the large separations for these four models, we used the fact that the averaged asymptotic large separations follow a homologous relation of the type

$$\langle \Delta\nu_{n,l} \rangle = C_\nu \cdot (M/M_\odot)^{1/2} (R/R_\odot)^{-3/2}. \quad (10)$$

The value of  $C_\nu$  for our reference model of  $\alpha$  Cir is  $130.8 \mu\text{Hz}$ . In Table 6 we list the masses of these models, as derived from CESAM evolution tracks using the same input parameters as for our reference model, their radii, as derived from their luminosities and effective temperatures, and the corresponding large separations, derived through the homologous scaling in Eq. (10).

Inspection of Table 6 shows that the large separations of the models ( $59$  to  $65 \mu\text{Hz}$ ) agree well with the observed value ( $60 \mu\text{Hz}$ ). However, this is not the case for the high effective temperatures that have been suggested in the literature (see Paper I for a discussion). For an effective temperature of  $7900$  K, and with a similar luminosity and mass, using the homologous scaling in Eq. (10) we find that the large separation of the model is about  $75 \mu\text{Hz}$ , greatly exceeding the observed value. Hence, the astero-

**Table 6.** Masses, radii and average large separations obtained from the homologous scaling given for models A, B, C, and D shown in Fig. 8.

model	$M/M_{\odot}$	$R/R_{\odot}$	$\langle \Delta\nu_{n,l} \rangle$ [ $\mu\text{Hz}$ ]
A	1.742	1.93	64
B	1.715	2.03	59
C	1.685	2.00	60
D	1.715	1.90	65

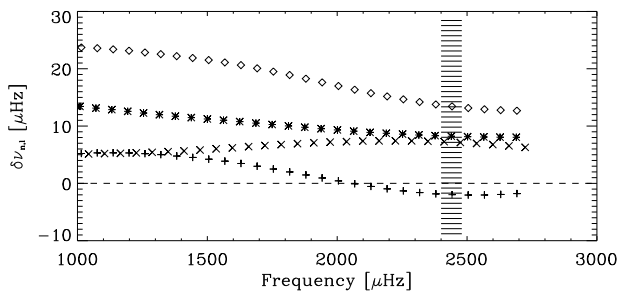


**Figure 9.** The frequency differences defined by Eq. (11) are shown versus mode frequency. Results are given for the cases when the triplet is assumed to involve modes of degrees  $l = 1, 0, 1$  (plus symbols),  $l = 2, 1, 2$  (crosses),  $l = 3, 2, 3$  (asterisks), and  $l = 3, 0, 3$  (diamonds). The observed value is marked by the horizontal dashed line and the hatched region marks the location of the triplet.

seismic modelling of the observed large separation strongly supports the effective temperature derived for  $\alpha$  Cir in Paper I.

### 5.3 Evidence for magnetic perturbation of the modes

Despite the general agreement found between the observed and computed large separations, there are aspects about the observed frequencies that cannot be accounted for with the models considered here. Firstly, only the frequencies  $f_6$ ,  $f_1$  and  $f_7$  seem to follow a regular frequency pattern. In particular, the low amplitude mode  $f_4$ , which is seen in both the *WIRE* data presented in this paper and the data acquired by Kurtz et al. (1994), is offset by about a quarter of the large separation from where it would be expected, according to the asymptotic approximation. Moreover, the almost-equal value of the separations  $(f_1 - f_6)$  and  $(f_7 - f_1)$  is also not reproduced by the reference model. If the triplet is assumed to correspond to modes of alternating parity and adjacent orders, then the difference between these two frequency separations can be written

$$\delta\nu_{n,l} \equiv 2\nu_{n,l} - \nu_{n-1,l+1} - \nu_{n,l+1}. \quad (11)$$

Under the same conditions as those required for Eq. (9) to be valid,  $\delta\nu_{n,l}$  is asymptotically given by (e.g. Cunha et al. 2007)

$$\delta\nu_{n,l} \simeq -4(l+1) \frac{\Delta\nu_0}{4\pi^2\nu_{n,l}} \int_0^R \frac{dc}{dr} \frac{dr}{r}. \quad (12)$$

Given the increase of the sound speed with depth in the star,  $\delta\nu_{n,l}$  is expected to be positive, increasing proportionally to  $(l+1)$ .

The observed value for this quantity is  $\delta\nu_{\text{obs}} \equiv -((f_7 - f_1) - (f_1 - f_6)) = 0.0039 \pm 0.0014 \mu\text{Hz}$ . In Fig. 9 we plot  $\delta\nu_{n,l}$  for our reference model (cf. Table 5), assuming different combinations of the degrees of the modes in the triplet:  $l = (1, 0, 1)$ ,  $l = (2, 1, 2)$ ,  $l = (3, 2, 3)$ , and  $l = (3, 0, 3)$ . In the last case  $\delta\nu_{n,l}$  is defined in a

similar way, but with  $(n-1, l+1)$  and  $(n, l+1)$  replaced by  $(n-2, l+3)$  and  $(n-1, l+3)$ , respectively. Except for the combination  $l = (1, 0, 1)$ , the values of  $\delta\nu_{n,l}$  are positive and increase with  $l$ , as expected from the asymptotic expression. The deviation of  $\delta\nu_{n,l}$  from the expected trend in the case of alternating modes of degrees  $l = 1, l = 0$  and  $l = 1$  is not surprising, since in the asymptotic analysis leading to Eqs. (9) and (12) it is assumed that the sound speed varies smoothly with depth. Because A-type stars have convective cores, that assumption breaks down at the edge of the core. The modes of lowest degree, which propagate deeper, will feel the effect of that rapid variation in the sound speed, and thus, their relative frequency is likely to deviate more strongly from the asymptotic behavior.

Regardless of how closely the quantity  $\delta\nu_{n,l}$  derived from our model follows the asymptotic behavior expressed by Eq. (12), it is clear that for all possible combinations of modes considered, this quantity is significantly different from the observed value (dashed horizontal line in Fig. 9) in the region where the modes are observed (the hatched region from 2.4 to 2.5 mHz). The smallest absolute value found for the theoretical  $\delta\nu_{n,l}$  in the range of the observed frequencies, is around  $2.0 \mu\text{Hz}$  for  $l = (1, 0, 1)$ , which is much larger than the  $3.9 \text{ nHz}$  determined from the observations. Considering modes of degree higher than  $l = 3$  will not solve this discrepancy, since  $\delta\nu_{n,l}$  will increase with increasing  $l$ . Moreover, we find that this discrepancy is also present for models A, B, C, and D, i.e. none of our theoretical calculations can explain the almost-equal separation observed between the three frequencies  $f_6$ ,  $f_1$  and  $f_7$ . It remains to be investigated whether the effect of the magnetic field, which has been ignored in the models considered so far, may explain this and the other apparent disagreements between theoretical and observed quantities discussed here.

The effect of the magnetic field on the pulsations of roAp stars has been studied by different authors for over a decade (Dziembowski & Goode 1996; Bigot et al. 2000; Cunha & Gough 2000; Saio & Gautschi 2004; Cunha 2006; Sousa & Cunha 2008). However, it is only recently that magnetic models have started to be used, in a forward approach, in an attempt to fit the asteroseismic data of particular pulsators (Gruberbauer et al. 2008; Huber et al. 2008). The study of pulsations in the presence of a magnetic field is a complex one. In order to make it treatable, a number of assumptions and approximations have to be introduced. Thus, quantitative comparisons between observed frequencies and frequencies derived from magnetic models require some caution. Nevertheless, there are a number of robust results derived from the magnetic models that one may confidently use. Cunha (2005) argued that the effect of a dipolar magnetic field is always to increase the large separation by a small amount, that can vary from nearly zero to a few  $\mu\text{Hz}$ . Since our non-magnetic models reproduce well the observed large separation, we expect that in the case of  $\alpha$  Cir the change in the large separation when including the magnetic field will be relatively small. On the other hand, a detailed magnetic modelling of  $\alpha$  Cir is necessary to test whether the effects produced by a magnetic field with properties consistent with the observational constraints may remove the discrepancies found between our models and the observed value of  $\delta\nu_{n,l}$ , as well as explain the deviation from the asymptotic trend of some of the observed oscillation frequencies. Such analysis will be presented in a separate paper (Brandão et al., in preparation).

Finally, we would like to emphasize that the almost-equal separation of the modes that compose the main triplet raises a question that goes beyond the simple issue of whether a particular magnetic field may bring the model predictions into agreement with the ob-

servations. In fact, even if such a magnetic field is found, its effect will depend on the frequency and so a precise cancellation of the difference  $(f_7 - f_1) - (f_1 - f_6)$  may occur only in a very particular range of frequencies. Therefore, the question of whether there is an underlying reason for the principal modes to be found precisely in that range of frequencies, must also be considered. In particular, model simulations that provide a measurement of how often this precise cancellation is expected to occur need to be carried out, and compared with the empirical evidence from observations of other multi-periodic roAp stars.

#### 5.4 The *Hipparcos* and asteroseismic parallaxes

Prior to the *WIRE* observations presented in this paper, the pattern of observed frequencies observed in  $\alpha$  Cir by Kurtz et al. (1994) suggested a large separation of  $50 \mu\text{Hz}$ . Matthews et al. (1999) used this value, together with an effective temperature of  $T_{\text{eff}} = 8000 \text{ K}$  and a mass of  $M = 2.0 \pm 0.5 M_{\odot}$  to calculate the expected “asteroseismic” parallax of  $\alpha$  Cir. The value they determined,  $\pi_{\text{ast}} = 51.3 \pm 1.2$ , was significantly smaller ( $7\sigma$ ) than the parallax measurement by *Hipparcos* ( $\pi_{\text{Hip-97}} = 60.97 \pm 0.58 \text{ mas}$ ; Perryman & ESA 1997). Moreover, a similar calculation for another 11 roAp stars indicated that the *Hipparcos* parallaxes were systematically larger than the parallaxes derived from the asteroseismic data of these roAp stars. The new, higher value for the large separation found in this paper, together with the lower mass and  $T_{\text{eff}}$  from Paper I, resolve the discrepancy found for  $\alpha$  Cir. Using Eq. (4) from Matthews et al. (1999) we derive a luminosity of  $\alpha$  Cir of  $L = 10.6 \pm 1.5 L_{\odot}$ . We adopt a mass of  $M = 1.7 \pm 0.2 M_{\odot}$  and  $T_{\text{eff}} = 7420 \pm 170 \text{ K}$  (both values from Paper I), a bolometric correction of  $BC = 0.19 \pm 0.08$  (Brandão et al. 2007; average of their two estimates),  $M_{\text{bol},\odot} = 4.75$ ,  $V = 3.19$ , and  $E(B - V)_{\text{max}} = 0.06 \pm 0.02$  (from Matthews et al. 1999) to get  $\pi_{\text{ast}} = 62.8 \pm 5.3 \text{ mas}$ . This is in good agreement with the parallax from *Hipparcos*, which was recently updated to  $\pi_{\text{Hip-07}} = 60.36 \pm 0.14 \text{ mas}$  (van Leeuwen 2007). This resolves the problem of the low asteroseismic parallax for  $\alpha$  Cir found by Matthews et al. (1999). Moreover, the lower effective temperature of  $\alpha$  Cir found in Paper I corroborates one of the suggestions of Matthews et al. (1999), namely that the systematic discrepancy between the asteroseismic and *Hipparcos* parallaxes could be associated with a systematic error in the determination of the effective temperatures of roAp stars.

In Fig. 10 we plot the *Hipparcos* parallaxes versus the asteroseismic parallaxes for eight roAp stars. This is an update of the original Fig. 1 from Matthews et al. (1999). Four stars are omitted (HD 119027, 166473, 190290, and 203932) because the uncertainty on their *Hipparcos* parallax is 8–10 times larger than for the other stars. For  $\alpha$  Cir we used the values found above, and for the other stars we used the information in Tables 1 and 2 of Matthews et al. (1999) and updated parallaxes from van Leeuwen (2007). Note that we have adopted larger uncertainties on  $T_{\text{eff}}$  ( $\sigma_T = 200 \text{ K}$ ) and on mass ( $\sigma_M = 0.5 M_{\odot}$ ). The solid line in Fig. 10 shows equality, and it seems that there is now acceptable agreement for most stars, the exceptions being HD 217522 and HD 137949.

## 6 CONCLUSIONS

We have analysed observations of the roAp star  $\alpha$  Cir, comprising 84 days of photometric time series from the star tracker on the

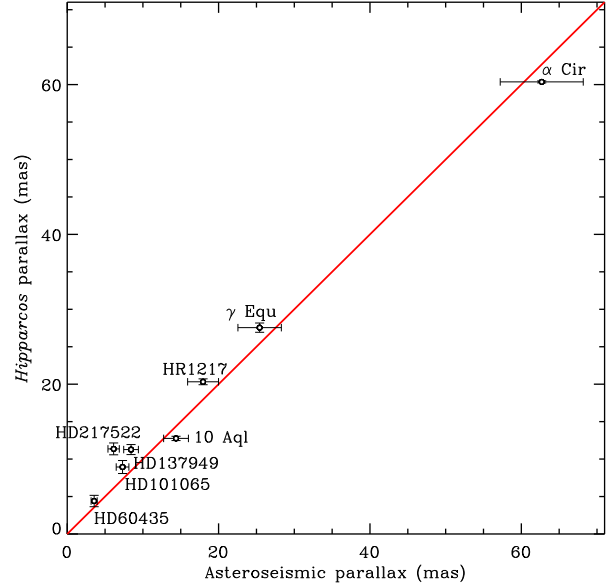


**Figure 10.** The *Hipparcos* parallaxes of eight roAp stars are plotted vs. the asteroseismic parallaxes as determined from the large separation,  $T_{\text{eff}}$ , and mass. This is an updated version of Fig. 1 from Matthews et al. (1999).

*WIRE* satellite. We used data from four different runs lasting between 8 and 42 days collected over six years, or nearly the entire mission life time of *WIRE* (Bruntt & Southworth 2008).

The four light curves from *WIRE* all show a double wave modulation with a period of  $P_{\text{rot}} = 4.4792 \pm 0.0004 \text{ d}$  and a peak-to-peak amplitude of 4 mmag. We interpret this variation as being due to spots on the surface giving us directly the rotation period of the star. This is the first direct detection and was only made possible with the very stable photometry – on both short and long timescales – from *WIRE*. Interestingly, the amplitude and phase of the modulation did not change significantly from 2000 to 2006 and hence the spot configuration seems to be extremely stable. The rotation period confirms an earlier indirect detection by Kurtz et al. (1994). Our initial assessment is that the spots need to be equatorial to explain the double wave rotational light curve, hence – unusually for an Ap star – the spots are not associated with the single, visible magnetic pole. Further study of the rotational light variation is in progress.

At much shorter periods (7 minutes) we detect the known dominant mode of pulsation at 2442 mHz; in addition, we have discovered two new frequencies located symmetrically around the principal mode. This triplet of frequencies is detected in the two runs from 2006, but not in the first two runs in 2000 and 2005. This is not due to differences in detection sensitivity, therefore the new frequencies must have appeared sometime between 2005 and 2006. This new discovery is confirmed by our ground-based photometry during 16 nights from SAAO, collected simultaneously with the two *WIRE* runs in 2006. The separation of the peaks is  $\Delta f_{\text{obs}} = 30.173 \pm 0.004 \mu\text{Hz}$ . Based on our theoretical models of  $\alpha$  Cir we interpret this as half the large separation, meaning that the triplet consists of modes with spherical degree of alternating parity. To confirm that our interpretation is correct will require that one or more frequencies with this separation are observed.

The principal mode has symmetrical sidelobes with a frequency separation equal to the rotational frequency,  $f_{\text{rot}} =$

2.58  $\mu$ Hz. We find that at the rotational phase of pulsation amplitude maximum, the pulsation phases of the three frequencies are equal within uncertainties. In the framework of the oblique rotator model this is expected when the pulsation axis and the rotation axis are not aligned. Thus, the three frequencies describe the change in observed pulsation amplitude as the observer views the deformation of the star from different perspectives. We have used the ratio of the amplitudes of the rotational frequency triplet to test different possibilities for the spherical degree and azimuthal order of the principal mode. We conclude that only modes with observational properties similar to those of a mode with  $l = 1, m = 0$  agree with the observations. This could be the dipole mode itself, or it could be a mode of higher degree that is distorted by the magnetic field such that a dipolar component dominates the observed rotational amplitude modulation.

We have computed models that are consistent with the fundamental parameters of  $\alpha$  Cir using as constraints the interferometric radius and the effective temperature from Paper I. For the first time in the study of  $\alpha$  Cir, the theoretical large separations derived from the models are in good agreement with the observations. The separations between the observed modes in the triplet  $f_6 + f_1 + f_7$  differ by only 3.9 nHz and this cannot be reconciled with the theoretical calculations presented in this work. We have discussed that magnetic effects may possibly account for this discrepancy but postpone the detailed analysis to a future publication (Brandão et al., in preparation).

We have compared the *Hipparcos* parallax of  $\alpha$  Cir with the value inferred from the large separation, assuming our interpretation above is correct. We find good agreement and this seems to resolve the issue of the discrepant value for  $\alpha$  Cir as discussed by Matthews et al. (1999).

## ACKNOWLEDGMENTS

This research has been funded by the Australian Research Council. DWK acknowledges support for this work from the UK Science and Technology Facilities Council (STFC). MC is supported by the Ciencia2007 Programme from FCT (C2007-CAUP-FCT/136/2006) and by FCT and FEDER (POCI2010) through the projects PDCTE/CTE-AST/81711/2006 and PTDC/CTE-AST/66181/2006. IMB is supported by FCT through the grant SFRH/BD/41213/2007. GH is supported by the Austrian "Fonds zur Förderung der wissenschaftlichen Forschung" under grants P18339-N08 and P20526-N16. IMB is very grateful to João Pedro Marques for providing useful material in relation to the theoretical models. We thank Vladimir Elkin for providing a high-precision measurement of  $v \sin i$  for  $\alpha$  Cir. Part of this work was supported by the European Helio- and Asteroseismology Network (HELAS), a major international collaboration funded by the European Commission's Sixth Framework Programme. This research has made use of the SIMBAD database, operated at CDS, Strasbourg, France.

## REFERENCES

Balmforth N. J., Cunha M. S., Dolez N., Gough D. O., Vauclair S., 2001, *MNRAS*, 323, 362  
 Balona L. A., Laney C. D., 2003, *MNRAS*, 344, 242  
 Bigot L., Dziembowski W. A., 2002, *A&A*, 391, 235

Bigot L., Provost J., Berthomieu G., Dziembowski W. A., Goode P. R., 2000, *A&A*, 356, 218  
 Brandão I. M., Cunha M. S., Gameiro J. F., 2007, *ArXiv e-prints*, 712  
 Bruntt H., 2007, *Communications in Asteroseismology*, 150, 326  
 Bruntt H., Kjeldsen H., Buzasi D. L., Bedding T. R., 2005, *ApJ*, 633, 440  
 Bruntt H., North J. R., Cunha M., Brandão I. M., Elkin V. G., Kurtz D. W., Davis J., Bedding T. R., Jacob A. P., Owens S. M., Robertson J. G., Tango W. J., Gameiro J. F., Ireland M. J., Tuthill P. G., 2008, *MNRAS*, 386, 2039 (Paper I)  
 Bruntt H., Southworth J., 2008, *Journal of Physics Conference Series*, 118, 012012  
 Bruntt H., Stello D., Suárez J. C., Arentoft T., Bedding T. R., Bouzid M. Y., Csubry Z., Dall T. H., Dind Z. E., Frandsen S., Gilliland R. L., 2007, *MNRAS*, 378, 1371  
 Buzasi D., 2002, in Aerts C., Bedding T. R., Christensen-Dalsgaard J., eds, *IAU Colloq. 185: Radial and Nonradial Pulsations as Probes of Stellar Physics ASP Conf. Series 259, Asteroseismic Results from WIRE (invited paper)*. p. 616  
 Bychkov V. D., Bychkova L. V., Madej J., 2005, *A&A*, 430, 1143  
 Christensen-Dalsgaard J., 2008, *Ap&SS*, p. 1  
 Cunha M. S., 2001, *MNRAS*, 325, 373  
 Cunha M. S., 2002, *MNRAS*, 333, 47  
 Cunha M. S., 2005, *JA&A*, 26, 213  
 Cunha M. S., 2006, *MNRAS*, 365, 153  
 Cunha M. S., 2007, *Communications in Asteroseismology*, 150, 48  
 Cunha M. S., Aerts C., Christensen-Dalsgaard J., Baglin A., Bigot L., Brown T. M., Catala C., Creevey O. L., Domiciano de Souza A., Eggenberger P., Garcia P. J. V., Grundahl F., Kervella P., Kurtz D. W., 2007, *A&A Rev.*, 14, 217  
 Cunha M. S., Fernandes J. M. M. B., Monteiro M. J. P. F. G., 2003, *MNRAS*, 343, 831  
 Cunha M. S., Gough D., 2000, *MNRAS*, 319, 1020  
 Dziembowski W. A., Goode P. R., 1996, *ApJ*, 458, 338  
 Gruberbauer M., Saio H., Huber D., Kallinger T., Weiss W. W., Guenther D. B., Kuschnig R., Matthews J. M., Moffat A. F. J., Rucinski S., Sasselov D., Walker G. A. H., 2008, *A&A*, 480, 223  
 Huber D., Saio H., Gruberbauer M., Weiss W. W., Rowe J. F., Hareter M., Kallinger T., Reegen P., Matthews J. M., Kuschnig R., Guenther D. B., Moffat A. F. J., Rucinski S., Sasselov D., Walker G. A. H., 2008, *A&A*, 483, 239  
 Hubrig S., Kurtz D. W., Bagnulo S., Szeifert T., Schöller M., Mathys G., Dziembowski W. A., 2004, *A&A*, 415, 661  
 Hubrig S., North P., Schöller M., 2007, *Astronomische Nachrichten*, 328, 475  
 Kupka F., Bruntt H., 2001, Using TEMPLOGG for determining stellar parameters of MONS targets. First COROT/MONS/MOST Ground Support Workshop, p. 39  
 Kupka F., Ryabchikova T. A., Weiss W. W., Kuschnig R., Rogl J., Mathys G., 1996, *A&A*, 308, 886  
 Kurtz D. W., 1982, *MNRAS*, 200, 807  
 Kurtz D. W., 1985, *MNRAS*, 213, 773  
 Kurtz D. W., Balona L. A., 1984, *MNRAS*, 210, 779  
 Kurtz D. W., Cropper M. S., 1981, *Informational Bulletin on Variable Stars*, 1987, 1  
 Kurtz D. W., Elkin V. G., Mathys G., 2005, *MNRAS*, 358, L6  
 Kurtz D. W., Elkin V. G., Mathys G., 2006a, in *Proceedings of SOHO 18/GONG 2006/HELAS I, Beyond the spherical Sun Vol. 624 of ESA Special Publication, Observations of magnetoacoustic modes in strongly magnetic pulsating roAp stars*

- Kurtz D. W., Elkin V. G., Mathys G., 2006b, *MNRAS*, 370, 1274
- Kurtz D. W., Elkin V. G., Mathys G., Riley J., Cunha M. S., Shibahashi H., Kambe E., 2004, in Zverko J., Ziznovsky J., Adelman S. J., Weiss W. W., eds, *The A-Star Puzzle Vol. 224 of IAU Symposium, Some recent discoveries in roAp stars*. p. 343
- Kurtz D. W., Kanaan A., Martinez P., Tripe P., 1992, *MNRAS*, 255, 289
- Kurtz D. W., Martinez P., 2000, *Baltic Astronomy*, 9, 253
- Kurtz D. W., Shibahashi H., 1986, *MNRAS*, 223, 557
- Kurtz D. W., Shibahashi H., Goode P. R., 1990, *MNRAS*, 247, 558
- Kurtz D. W., Sullivan D. J., Martinez P., Tripe P., 1994, *MNRAS*, 270, 674
- Lenz P., Breger M., 2005, *Communications in Asteroseismology*, 146, 53
- Matthews J. M., Kurtz D. W., Martinez P., 1999, *ApJ*, 511, 422
- Montgomery M. H., O'Donoghue D., 1999, *Delta Scuti Star Newsletter*, 13, 28
- Morel P., 1997, *A&AS*, 124, 597
- Netopil M., Paunzen E., Maitzen H. M., North P., Hubrig S., 2008, *A&A*, 491, 545
- Perryman M. A. C., ESA eds, 1997, *The HIPPARCOS and TYCHO catalogues. Astrometric and photometric star catalogues derived from the ESA HIPPARCOS Space Astrometry Mission Vol. 1200 of ESA Special Publication*
- Pyper D. M., 1969, *ApJS*, 18, 347
- Roberts P. H., Soward A. M., 1983, *MNRAS*, 205, 1171
- Rogers N. Y., 1995, *Communications in Asteroseismology*, 78, 1
- Ryabchikova T., Sachkov M., Kochukhov O., Lyashko D., 2007, *A&A*, 473, 907
- Saio H., 2005, *MNRAS*, 360, 1022
- Saio H., Gautschi A., 2004, *MNRAS*, 350, 485
- Shibahashi H., 1986, in Osaki Y., ed., *Hydrodynamic and Magnetodynamic Problems in the Sun and Stars Asteroseismology*. p. 195
- Shibahashi H., Takata M., 1993, *PASJ*, 45, 617
- Sinachopoulos D., 1989, *A&AS*, 81, 103
- Sousa S. G., Cunha M. S., 2008, *MNRAS*, 386, 531
- Takata M., Shibahashi H., 1995, *PASJ*, 47, 219
- Tassoul M., 1980, *ApJS*, 43, 469
- van Leeuwen F., 2007, *Hipparcos, the New Reduction of the Raw Data. Astrophysics and Space Science Library*, Springer

This paper has been typeset from a  $\text{T}_{\text{E}}\text{X}/\text{L}^{\text{A}}\text{T}_{\text{E}}\text{X}$  file prepared by the author.